A Comparison of Optimized Mitigation Techniques for Swept-frequency Jammers

Wenjian Qin, Fabio Dovis, *Politecnico di Torino, Torino, Italy*
Micaela Troglia Gamba, Emanuela Falletti, *LINKS Foundation, Torino, Italy*

BIOGRAPHY

Wenjian Qin received his B.E degree and M.S degree in Geomatics respectively from Wuhan University, China and University of Stuttgart, Germany. He is currently a PhD student at the Department of Electronics and Telecommunications of Politecnico di Torino, Italy. His research field covers GNSS interference detection and mitigation technology.

Fabio Dovis is an associate professor at the Department of Electronics and Telecommunications of Politecnico di Torino as a member of the Navigation Signal Analysis and Simulation (NavSAS) group. His research interests cover the design of GPS and Galileo receivers and advanced signal processing for interference and multipath detection and mitigation. He has a relevant experience in European projects in satellite navigation as well as cooperation with industries and research centers.

Micaela Troglia Gamba received the Co-tutelle Ph.D. in Electronics and Communication Engineering from Politecnico di Torino and Télécom Bretagne, France, in 2011. She is currently a researcher in the Navigation Technologies area of LINKS Foundation Torino, Italy. She mainly works as Software Designer and Developer, mainly focusing on digital signal processing techniques and interference detection and mitigation algorithms.

Emanuela Falletti is the head of the GNSS Core Algorithms unit of the LINKS Foundation. She holds a Ph.D. degree in Electronics and Communications Engineering. Her research activity focuses on digital signal processing and simulation techniques for GNSS software receivers, including signal quality monitoring, interference and spoofing monitoring, multi-antenna processing.

ABSTRACT

This paper proposes an optimization of the characteristic parameters that define four architectures of adaptive notch filters, used to mitigate the effect of swept-frequency (chirp) jamming signals at the input of a GNSS receiver. The optimization is based on a performance metric computed at the acquisition stage of the receiver that represents a measure of the ratio between the peak of the cross-ambiguity function computed in acquisition and the noise floor. The optimization is intended to find the parameters of the adaptive notch filter architectures that minimize the loss in terms of this metric with respect to the interference-free case. The paper discusses the optimization of the parameters for the four considered architectures. The optimization process is performed under different working conditions, so as to highlight the sensitivity of the parameters to the changes of the operational scenarios. This paper presents the results of an analysis which is meant to evolve in a more complete picture of the optimal performance achievable by an adaptive notch filter in the presence of chirp jamming signals.

I. INTRODUCTION

The disruptive effect of Radio-Frequency Interference (RFI) on Global Navigation Satellite System (GNSS) receiver, and consequently on all GNSS-dependent applications, is well known and increasingly alarming [1]. Among the intentional sources of interference, today the jamming is one of the most feared GNSS impairments, able to disrupt GNSS-based services in wide geographical areas [2]. Jamming signals occurrence has been observed and reported in many recent newspaper and magazine articles [3]–[5], demanding for an increasing need of countermeasures [6].

Many techniques have been proposed so far in literature to detect, characterize, localize and mitigate jamming signals. The interested reader can refer to [7][8] for a comprehensive survey of the main state-of-the-art solutions. Among all of these, the well-

https://doi.org/10.33012/2019.16691

known Adaptive Notch Filter (ANF) is still far from being an outdated technique, despite widely explored in literature with many variations [9]–[11]. ANFs are effective for Continuous Wave Interference (CWI) [11][12], efficient for Narrow Band Interference (NBI) [13], and, more recently, its suitability in mitigating the effects of GNSS jammers has been also investigated and demonstrated [14][15]. Recently, a family of ANFs, where the adaptation block is modelled as a Frequency Lock Loop (FLL), has been analyzed in detail in [9] (FLL-equivalent ANFs) for an instructive study of performance of the adaptation capability. ANFs are appealing for low complexity, low computational cost and reduced activation time if compared with other more effective but also more complex solutions such as transform domain excision techniques [10]. Beyond the implementation aspects, the FLL equivalence mentioned above makes them particularly interesting since the adaptive capability of tracking time-varying interfering frequencies can be analyzed using the FLL theory, already widely employed in GNSS tracking loop analysis.

In our recent paper [15], we considered two FLL models proposed in [9] to implement the adaptive capability of the ANF: the standard FLL and the FLL with exponential filtering. While the former is equivalent to minimize the energy at the output of the Moving Average (MA) part of the notch filter, the latter corresponds to the minimization of the energy of the notch filter output. In particular, in [15] both have been evaluated in case of interference from fast swept-frequency jammers: while the standard FLL shows to be able to successfully track and mitigate jamming signals, the exponential filtering FLL proves it is not up to, suffering particularly from frequency discontinuities, which commonly characterize such kind of interferers.

With this work we aim at complementing and enriching the findings presented in [15], first providing an analysis of the distortion induced by the notch filter on the GNSS ranging code, second, pursuing an optimization of the ANF parameters aimed at minimizing such distortions, still preserving the interference mitigation capabilities of the filter. A preliminary work in this direction was conducted in [12], with the evaluation of correlation distortions in the GNSS signal tracking stage produced by a model of exponential-FLL ANF. In the current work, the principal key performance indicator of the ranging code distortion is the α_{mean} measured at the GNSS signal acquisition stage. In fact, it is well known that the jammers aim at blinding the GNSS receivers and blocking the acquisition stage. It is then important that any mitigation techniques not only remove the spurious power of the interference, but also improve as much as possible the detection probability of the GNSS signals by the receiver.

In acquisition, the incoming signal is correlated with a series of locally generated replicas until the acquisition detector crosses a predefined threshold, i.e. a correlation peak has been found in the search space. Based on this, the impact of interference on the acquisition stage can be evaluated by exploiting a figure of merit, namely α_{mean}, which is defined in [1] as the correlation peak-to-noise-floor ratio. As the interfering power increases, the value of α_{mean} decreases thus leading to an increasing probability of a false alarm [1]. When the ANF is adopted to mitigate the interference, e.g. jamming signals, the α_{mean}values can also be used to evaluate its filtering efficiency with different parameter settings at the acquisition stage. The parameter settings of ANF should be carefully tuned in order to enable the filter to successfully track and mitigate the jamming signals.

In the ANF, either in its regular [11] or FLL-equivalent representations [9][15], the pole contraction factor and algorithm step, respectively determining the width of the notch and the tracking capability of the filter, are the parameters that shape the interference mitigation capability of the ANF and should be carefully adjusted. The choice of a large value of the pole contraction factor (close to 1) ensures a narrow notch thus to keep the most useful GNSS signals after interference mitigation, but the side effect of this choice is the difficulty it induces to the adaptive criterion to track the frequency changes. On the other hand, the smaller the algorithm step is, the slowest the filter response to the interfering signal. Thus, a good trade-off between these parameters has to be addressed in order to allow such kind of filters not only to successfully mitigate the interference but also to preserve the useful GNSS signals as much as possible. Since the chirp signals generated by different jammers present various sweeping periods and bandwidths [16][17], it is always a tricky problem to customize proper parameter settings of the ANF to mitigate the specified chirp signals.

In this paper, the performance of the two main architectures (i.e. regular ANF [11] and FLL-equivalent ANFs [9][15]) and other new derived from the previous ones, have been evaluated and compared in case of swept-frequency jamming signal. The paper is organized as follows. In the next section, the methodology for distortion analysis based on α_{mean} is outlined and applied to the regular ANF architecture [11] as exemplary case, while its application to other ANF architectures, including the FLL-equivalent ones [9][15], is reported in Section III. The analysis is then completed in Section IV, showing the performance evaluation for different Jammer-to-Noise (J/N) and Jammer-to-Signal (J/S) ratios, focusing on the FLL models only. Finally, conclusions and practical considerations for a real implementation of the ANF are drawn in Section V.

II. METHODOLOGY FOR DISTORSION ANALYSIS

In order to investigate the optimization of the parameters with respect to the distortion and residual interference affecting the GNSS signal after filtering operation, the analysis is conducted for a special case of intentional interference: the swept-frequency jamming signal, characterized by a linear variation in frequency along time. In this section the theoretical model of the ANF is summarized and an optimization technique is proposed on the basis of α_{mean} values to configure the parameter settings of the ANF.

A. Theoretical Model of Adaptive Notch Filter

The approach of adaptive notch filtering based on Infinite Impulse Response (IIR) architecture has been extensively exploited to counteract GNSS interference with its benefit of low computational effort and satisfactory performance. As already proved in [18][19], in a baseband digital receiver working on the complex envelope representation of signals, an IIR one-pole notch filter can be adopted to mitigate a CWI, i.e. one spectral line at a certain frequency. According to [18][19] the z-domain transfer function of a notch filter is given by

$$H(z) = \frac{1 - z_0 z^{-1}}{1 - k_\alpha z_0 z^{-1}} \tag{1}$$

where z_0 is the zero placed in correspondence of the interference frequency to be canceled, and k_α is the pole contraction factor determining the width of the notch, with $0 \leq k_\alpha < 1$. The conversion between z_0 and the frequency of the filter notch f_0 is given by

$$z_0 = exp(j2\pi f_0 T_s) \tag{2}$$

where f_0 is expressed in units of cycle/second (Hz) and T_s is the sampling time of the input signal to the notch filter. Extended versions of the one-pole notch filter are the two-pole and multi-pole notch filters that allow to process a real input signal respectively with two or multiple spectra lines in the frequency domain [11].

The one-pole notch filter, described above, is particularly effective for the mitigation of CWI, assuming that only one interference with known frequency is present. The problem of detecting and tracking an interference, whose frequency is unknown and varies along the time, has been further addressed in [11][20] by introducing an adaptation algorithm to estimate the z_0 at run-time, according to the following Least-Mean-Square (LMS) iterative rule [11][20]

$$z_0[n] = z_0[n-1] - \mu[n] g(J[n]) \tag{3}$$

where all variables become function of the discrete time n. $g(J[n])$ is the stochastic gradient of the cost function $J[n]$, while $\mu[n]$ is the algorithm step. The adaptation algorithm makes use of the notch filter observables in order to make the z_0 estimate to converge toward the frequency of the interfering signal. As the frequency of the interference changes, the adaptation block will allow z_0 to progressively move in the complex plane and converge to the interference, thus allowing the filter to track the frequency variations of the interfering signal.

In order to properly define the cost function, the transfer function (1) can be written as a cascade of Auto Aggressive (AR) and MA filtering blocks and the cost function is then defined as a function of the observables of the AR and MA blocks. Based on [9], the transfer function (1) can be equivalently rewritten as

$$H_f(z) = 1 - z_0 z^{-1} \frac{1 - k_\alpha}{1 - k_\alpha z_0 z^{-1}} \tag{4}$$

where the transfer function of the AR part is explicitly written as

$$H_r(z) = \frac{1 - k_\alpha}{1 - k_\alpha z_0 z^{-1}} \tag{5}$$

and the corresponding input-output equation is

$$x_r[n] = (1 - k_\alpha) x[n] + k_\alpha z_0 x_r[n-1]. \tag{6}$$

The output of the MA part is given by

$$y_m[n] = x[n] - z_0 x[n-1]. \tag{7}$$

Then, the output of the ANF is obtained

$$x_f[n] = x[n] - z_0 x_r[n-1]. \tag{8}$$

According to [11][9], the cost function $J[n]$ can be either defined as the expectation of the energy of notch filter output $J[n] = E\{|x_f[n]|^2\}$ or the expectation of the energy of MA part $J[n] = E\{|y_m[n]|^2\}$, thus determining two different architectures of ANFs. The stochastic gradient of the cost function $g(J[n])$ in (3) is

$$g(J[n]) = \nabla_{z_0}(J[n]) \tag{9}$$

and the algorithm step $\mu[n]$ in (3) is given by

$$\mu[n] = \frac{\delta}{E\{|x_r[n]|^2\}} \tag{10}$$

where $E\{|x_r[n]|^2\}$ is the expectation of the energy of AR output and δ controls the convergence capability of the adaptation block.

Finally, the ANF is activated when the presence of interference is claimed by comparing the modulus of the averaged pole $|\hat{z}_0[n]|$ against an activation threshold T, with

$$\hat{z}_0[n] = a z_0[n-1] + (1-a) z_0[n] \tag{11}$$

where a is the forgetting factor of the moving average (11). The activation threshold T can be fixed by choosing a Jammer-to-Noise ratio, that can be considered harmful for the GNSS receiver.

Furthermore, considering the relationship in equation (2), the adaptation algorithm can also be designed on the basis of f_0 [9], i.e.,

$$f_0[n] = f_0[n-1] - \bar{\mu}[n]\bar{g}(J[n]) \tag{12}$$

with

$$\bar{\mu}[n] = \frac{\bar{\delta}}{E\{|x_r[n]|^2\}} \tag{13}$$

and

$$\bar{g}(J[n]) = \nabla_{f_0}(J[n]). \tag{14}$$

This adaptation algorithm based on f_0 is introduced for the purpose of comparing the regular ANF with the FLL-equivalent ANFs which will be discussed in Section III.

In Table 1, the abovementioned algorithms in the adaptation block are summarized and compared. Method 1 and method 2 directly update z_0 at each epoch, while method 3 and method 4 update f_0 first and afterwards derive z_0. These two different adaptation algorithms lead to different behavior of z_0. The former allows z_0 to move inside the unit circle during the transient time, while the latter keeps z_0 always on the unit circle due to the fact that f_0 is always a real value.

In this paper, for the sake of simplicity, only the difference on the choice of the cost function will be considered. Under this assumption, method 1 and method 3 merge, and so do method 2 and method 4. Furthermore, in this paper the method (1+3) with $J[n] = E\{|x_f[n]|^2\}$ and $g(J[n]) = \nabla_{z_0}(J[n])$ is referred to as "Regular ANF 1", while the method (2+4) with $J[n] = E\{|y_m[n]|^2\}$ and $\bar{g}(J[n]) = \nabla_{f_0}(J[n])$ is referred to as "Regular ANF 2", as listed in Table 2. These two methods will be further adopted to compare with the FLL-equivalent architecture.

Table 1. Comparison of algorithms for the adaptation block of the regular ANFs

Regular ANFs	**Method 1**	**Method 2**	**Method 3**	**Method 4**
Adaptation algorithm	$z_0[n] = z_0[n-1] - \mu[n]g(J[n])$.		$f_0[n] = f_0[n-1] - \bar{\mu}[n]\bar{g}(J[n])$ $z_0 = exp(j2\pi f_0 T_s)$	
Cost function	$J[n] = E\{\lvert x_f[n]\rvert^2\}$	$J[n] = E\{\lvert y_m[n]\rvert^2\}$	$J[n] = E\{\lvert x_f[n]\rvert^2\}$	$J[n] = E\{\lvert y_m[n]\rvert^2\}$
Stochastic gradient	$g(J[n]) = \nabla_{Z_0}(J[n])$		$\bar{g}(J[n]) = \nabla_{f_0}(J[n])$	
Algorithm step	$\mu[n] = \frac{\delta}{E\{\lvert x_r[n]\rvert^2\}}$		$\bar{\mu}[n] = \frac{\bar{\delta}}{E\{\lvert x_r[n]\rvert^2\}}$	

Table 2. Adaptation block of Regular ANF 1 and Regular ANF 2

Regular ANFs	**Regular ANF 1**	**Regular ANF 2**
Adaptation algorithm	$z_0[n] = z_0[n-1] - \mu[n]g(J[n])$.	$f_0[n] = f_0[n-1] - \bar{\mu}[n]\bar{g}(J[n])$ $z_0 = exp(j2\pi f_0 T_s)$
Cost function	$J[n] = E\{\lvert x_f[n]\rvert^2\}$	$J[n] = E\{\lvert y_m[n]\rvert^2\}$
Stochastic gradient	$g(J[n]) = \nabla_{Z_0}(J[n])$	$\bar{g}(J[n]) = \nabla_{f_0}(J[n])$
Algorithm step	$\mu[n] = \frac{\delta}{E\{\lvert x_r[n]\rvert^2\}}$	$\bar{\mu}[n] = \frac{\bar{\delta}}{E\{\lvert x_r[n]\rvert^2\}}$

B. Parameters Optimization Technique Based on α_{mean}

In the acquisition stage of a GNSS receiver, the incoming signal is correlated with a succession of locally generated replicas until the acquisition detector crosses a predefined threshold, i.e. a correlation peak has been found in the search space. Based on this, the impact of interference on the acquisition stage can be evaluated by exploiting a figure of merit, namely α_{mean}, which is defined in [1] as the correlation peak-to-noise-floor ratio, given by

$$\alpha_{mean} = 20\log_{10}\left(\frac{x_p}{E_i}\right) \tag{15}$$

where x_p is the correlation peak at the acquisition stage and E_i is the average of i off-peak correlation points in the acquisition search space.

The value of α_{mean} decreases as the interfering power increases, thus leading to an increasing probability of a false alarm [1]. The α_{mean} value can also be used to evaluate the ANF filtering efficiency as a function of different parameters. After the filtering operation, the cross correlation between the local replica and the input signal is distorted, and such effect on the ranging code is related to the optimization of the parameters. Different from other optimization methods proposed in literatures such as [21] to adjust the depth of the notch based on the overall signal-to-noise ratio, this method directly exploits the metric at the acquisition stage of a generic GNSS receiver, therefore in this way it is more customized in the sense of GNSS application and is easy to be implemented.

C. An Example of Parameters Optimization for the ANF

Hereafter we show the above presented methodology based on α_{mean} applied to the ANF algorithm illustrated in Subsection A. In particular, we simulated a scenario where a digital chirp jamming signal is generated and combined to a GPS L1 signal simulated by the N-FUELS Signal Generation Tool [22][23] at Intermediate Frequency (IF) and the ANF is exploited to track and mitigate the jamming signal. We reproduced a sampling rate of 40 MHz and $IF = 0$ Hz. In Figure 1 the spectrogram of the interfered signal is shown. The Sweeping Period (SP) of the chirp signal is $SP = 33$ μs which defines the time interval of one repetition of the chirp, while its bandwidth (frequency span) is 16 MHz. The power of the chirp signal is $P_{int} = -103$ dBW and Carrier-to-Noise ratio of the GPS signal is $C/N_0 = 55$ dB $-$ Hz. The parameters of the simulated chirp signal were chosen on the basis of a real jammer configuration, according to [17].

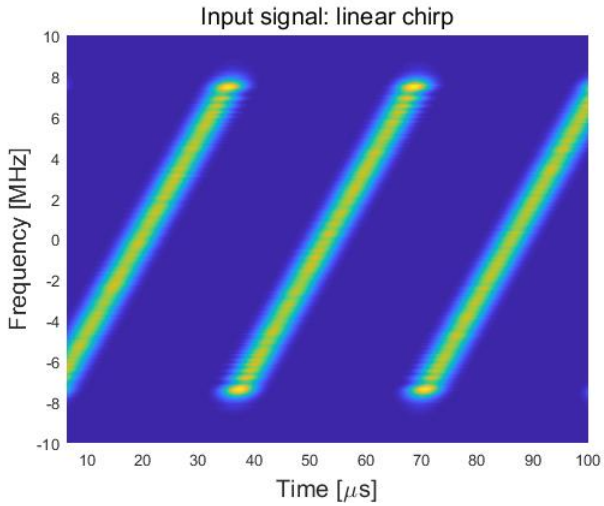

Figure 1. Spectrogram of the interfered signal.

As reference, the α_{mean} in case of interference-free signal is evaluated with $\alpha_{mean} = 46.8$ dB in this configuration. Hereafter the parameters of method Regular ANF 1 are optimized on the basis of the measurements of the α_{mean} performance indicator, in the presence of the jamming signal. The α_{mean} is calculated 50 times over 1 ms each and then averaged.

The optimization of the parameters k_α, δ and T is shown in Figure 2 and Figure 3, which illustrate the influence of the different parameter settings on the calculation of α_{mean}. As presented in Figure 2, with the threshold $T = 0.7$ and the forgetting factor $a = 0.9$, the α_{mean} values have significant variations with k_α when δ is between 0.05 and 0.2. The best trade-off between k_α and δ is to set $k_\alpha = 0.9$ and δ = 0.1. This configuration is effective due to the fact that the simulated jammer has a slow frequency rate and wide bandwidth, which makes the adaptation block have less difficulty to track the frequency variation, thus to allow a narrow notch (large value of k_α) to mitigate the interference. In Figure 3, with $\delta = 0.1$ and $a = 0.9$, the α_{mean} values are strongly dependent on the choice of k_α but rarely affected by T.

Thus, the aforementioned parameters are optimized by fixing k_α between 0.8 and 0.9, and δ between 0.1 and 0.15 on the basis of α_{mean} values. The threshold T can also be considered in order to finalize precise parameter settings, by tuning it as the minimum J/N considered harmful to the receiver. This is an example to demonstrate the procedure of parameters optimization for the ANF. Although in the scenario only three parameters are discussed, the trade-off based on the α_{mean} values can be also extended to other parameters of the ANF, such as the forgetting factor a in (11). The optimum α_{mean} value is still significantly lower than that obtained in the interference-free case, meaning that the jamming effect cannot be totally canceled out.

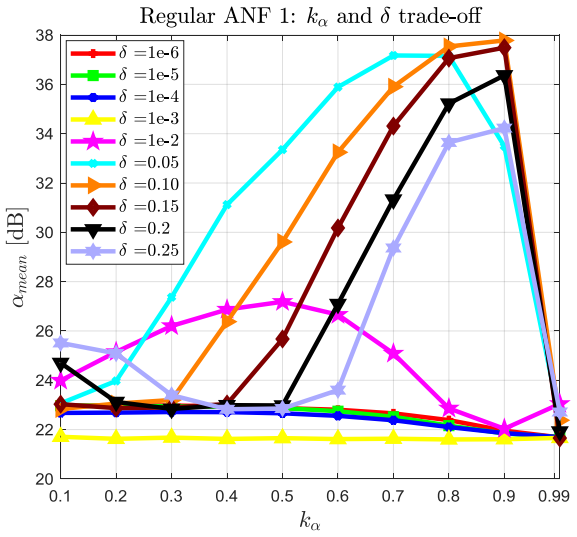

Figure 2. k_α and δ trade-off based on α_{mean}, with $T = 0.7$ and $a = 0.9$.

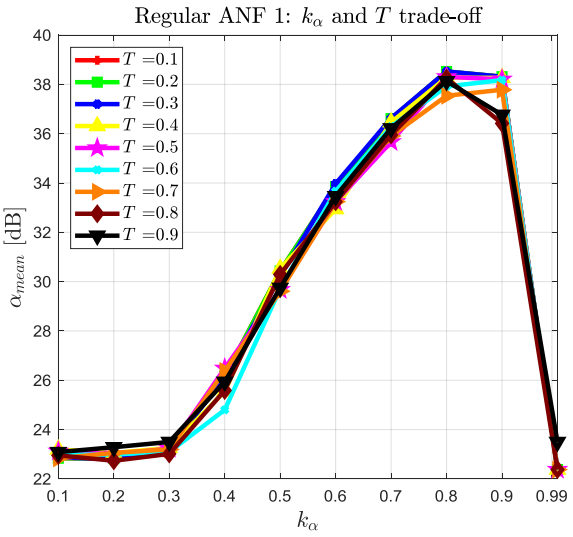

Figure 3. k_α and T trade-off based on α_{mean}, with $\delta = 0.1$ and $a = 0.9$.

Figure 4 shows the Cross-Ambiguity Function (CAF) of the interfered signal at the acquisition stage. Due to the strong interference, the power of the interference is distributed on the whole search domain, leading to a failure in the acquisition with $\alpha_{mean} = 21.6$ dB. After interference mitigation with a good combination of parameters achieved through the previous analysis, the acquisition is achieved with $\alpha_{mean} = 37.8$ dB as shown in Figure 5.

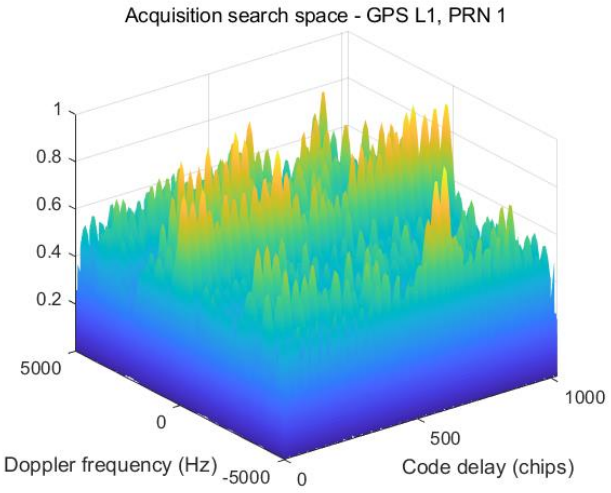

Figure 4. CAF of the interfered signal without interference mitigation. $\alpha_{mean} = 21.6$ dB.

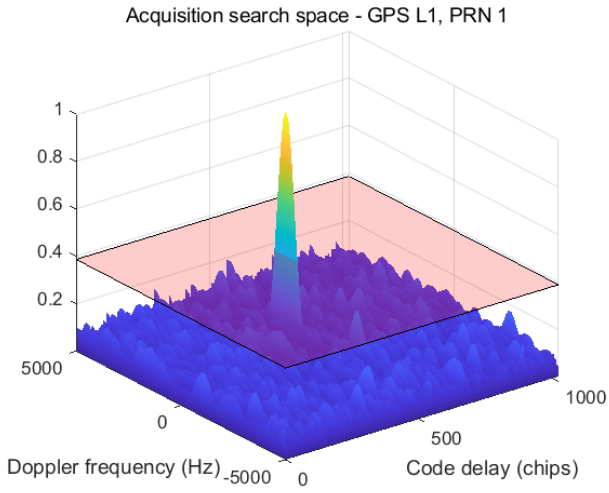

Figure 5. CAF of the mitigated signal, with $k_\alpha = 0.9$, $\delta = 0.1$, $T = 0.7$ and $a = 0.9$. $\alpha_{mean} = 37.8$ dB.

III. COMPARISON OF DIFFERENT ANF ARCHITECTURES

This section is intended to extend the concept of parameters optimization on the basis of α_{mean} as introduced in Section II to the case of FLL-equivalent ANFs and compare the results of the two families of ANF architectures, i.e. regular ANFs and FLL-equivalent ANFs. The major difference between the two architectures is the adaptation block: the algorithms for the FLL-equivalent ANFs are summarized in the following and the comparison between the regular ANFs and the first-order FLL-equivalent ANFs are given.

A. Theoretical Analysis

In [9], the equivalence between the adaptation block for the regular ANFs and the adaptation block for FLL-equivalent ANFs are established, which allow the adaptation block of the regular ANFs to be realized in either standard FLL or FLL with exponential filtering schemes. Similar to Regular ANF 1, the FLL with exponential filtering corresponds to the minimization of the energy of the notch filter output, while, similar to Regular ANF 2, the standard FLL is equivalent to minimize the energy at the output of the MA part. A further investigation on the performance of FLL-equivalent ANFs is presented in [15] which exploits dynamic stress error and noise jitter as the metrics to evaluate their performance on the mitigation of frequency-swept jamming signals. The results reflect that the standard FLL is able to successfully track frequency changes and to quickly react to the frequency discontinuities. On the contrary, the exponential filtering FLL proves to suffer particularly from frequency discontinuities, which commonly characterize the swept-frequency interferers.

Similar to (12), in the case of first-order FLL-equivalent ANFs, the f_0 is obtained through

$$f_0[n] = f_0[n-1] - \bar{v}\bar{g}(J[n]) \tag{16}$$

where the algorithm step $\bar{v}$ is the coefficient of the first-order loop filter in FLL. In Table 3 the mathematical expressions of the two FLL-equivalent ANFs are compared. According to [24] and [9], the algorithms to calculate $\bar{v}$ in the two FLL-equivalent ANFs are reported. In the standard FLL, $\bar{v}$ is a function of the bandwidth (B_n) of the loop filter in FLL, while in the exponential filtering FLL, $\bar{v}$ is a function of both B_n and k_α.

Table 3. Comparison on algorithms in the adaptation block between two FLL-equivalent ANFs

FLL-equivalent ANFs	Exponential filtering FLL	Standard FLL
Cost function	$J[n] = E\{\|x_f[n]\|^2\}$	$J[n] = E\{\|y_m[n]\|^2\}$
Stochastic gradient	$\bar{g}(J[n]) = \nabla_{f_0}(J[n])$	$\bar{g}(J[n]) = \nabla_{f_0}(J[n])$
Algorithm step	$\bar{v}(B_n, k_\alpha)$	$\bar{v}(B_n)$

In order to ease the comparison, the mathematical expressions that define the architectures of regular ANFs and FLL-equivalent ANFs are gathered in Table 4, as a summary of Table 2 and Table 3. Table 4 highlights that the difference between each regular ANF and its corresponding FLL-equivalent is the computation of the algorithm step. In the regular ANFs, $\mu[n]$ and $\bar{\mu}[n]$ are derived at each time instant n based on the output energy of the AR output, while the configurable parameters are δ and $\bar{\delta}$, which determine the tracking capability of the adaptation block. In the FLL-equivalent ANFs $\bar{v}$ is the coefficient of the loop filter in FLL and it is a function of the loop bandwidth B_n in the case of standard FLL as well as B_n and k_α in the case of exponential filtering FLL. The loop bandwidth B_n is a configurable parameter which determines the tracking capability of the FLL-equivalent architecture [15]. Consequently, the four architectures, although pairwise equivalent, differ for the parameters that can be subject of optimization and therefore may differ in the optimized performance.

B. Performance Comparison

In FLL-equivalent ANFs, similar to the regular ANF, k_α is the pole contraction factor to determine the width of the notch, while the loop bandwidth B_n plays a similar role as the algorithm step, i.e. δ and $\bar{\delta}$ in the regular ANFs, thus shaping the tracking capability of the filter. With a wider bandwidth, the FLL could better track the frequency variation, but also suffer from more noise entering the system. In a similar way, parameters of the FLL-equivalent ANFs can also be optimized with respect to the α_{mean} achieved after interference mitigation at the acquisition stage. The Regular ANF 1 and Regular ANF 2 methods are implemented and optimized for comparison with the FLL-equivalent structures.

Table 4. Comparison between the regular ANFs and the first-order FLL-equivalent ANFs in the adaptation block

ANF architectures	Regular ANF		First-order FLL-equivalent ANFs	
	Regular ANF 1	**Regular ANF 2**	**Exponential filtering FLL**	**Standard FLL**
Adaptation algorithm	$z_0[n] = z_0[n-1] - \mu[n]g(J[n])$	$f_0[n] = f_0[n-1] - \bar{\mu}[n]\bar{g}(J[n])$ $z_0 = exp(j2\pi f_0 T_s)$	$f_0[n] = f_0[n-1] - \bar{v}\bar{g}(J[n])$ $z_0 = exp(j2\pi f_0 T_s)$	
Cost function	$J[n] = E\{\lvert x_f[n]\rvert^2\}$	$J[n] = E\{\lvert y_m[n]\rvert^2\}$	$J[n] = E\{\lvert x_f[n]\rvert^2\}$	$J[n] = E\{\lvert y_m[n]\rvert^2\}$
Stochastic gradient	$g(J[n]) = \nabla_{z_0}(J[n])$	$\bar{g}(J[n]) = \nabla_{f_0}(J[n])$	$\bar{g}(J[n]) = \nabla_{f_0}(J[n])$	$\bar{g}(J[n]) = \nabla_{f_0}(J[n])$
Algorithm step	$\mu[n] = \frac{\delta}{E\{\lvert x_r[n]\rvert^2\}}$	$\bar{\mu}[n] = \frac{\bar{\delta}}{E\{\lvert x_r[n]\rvert^2\}}$	$\bar{v}(B_n, k_\alpha)$	$\bar{v}(B_n)$
Parameters under optimization	k_α, δ and T	k_α, $\bar{\delta}$ and T	k_α and B_n	k_α and B_n

The simulation scenario exploits the same interfered signal as the scenario in Section II and the four methods introduced in Table 4 are implemented to mitigate the interference. Figure 2 and Figure 6 show the optimization on the achieved α_{mean} values by Regular ANF 1 and exponential FLL, while Figure 7 and Figure 8 present the optimized α_{mean} values by Regular ANF 2 and standard FLL. With the optimized trade-off on the parameter settings of each method, the four methods could achieve comparable results. A further discussion on the performance of FLL-equivalent ANFs is presented in Section IV.

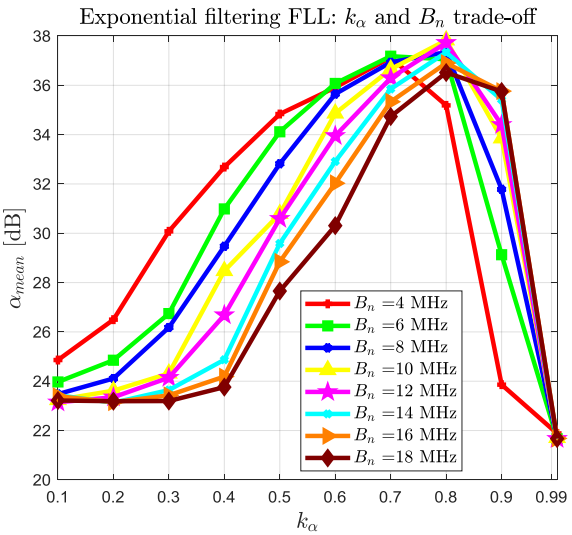

Figure 6. Exponential filtering FLL optimization, with the optimized trade-off: $k_\alpha = 0.8$, $B_n = 10$ MHz and $a = 0.9$.

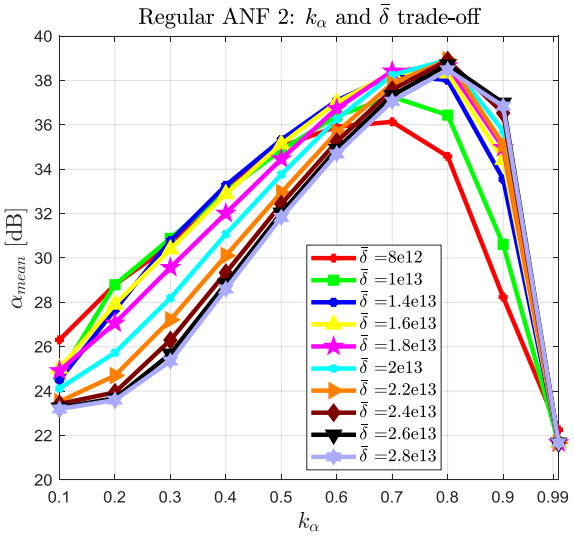

Figure 7. Regular ANF 2 optimization, with the optimized trade-off: $k_\alpha = 0.8$, $\delta = 2.4\text{e}13$, $T = 0.7$ and $a = 0.9$.

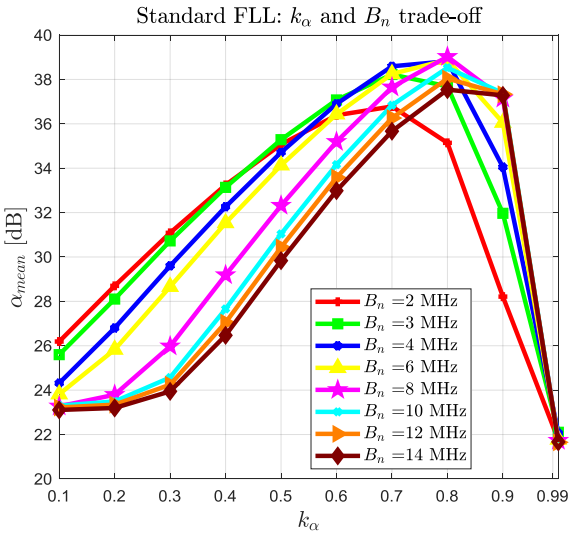

Figure 8. Standard FLL optimization, with the optimized trade-off: $k_\alpha = 0.8$, $B_n = 6$ MHz and $a = 0.9$.

IV. PERFORMANCE EVALUATION OF FLL-EQUIVALENT ANFS

In this section, the CAF distortion analysis, conducted in Sections II and III on the basis of the α_{mean} parameter for a case of strong jamming power, is completed for several values of Jammer-to-Noise ratio and Jammer-to-Signal conditions. Exploiting the equivalence of the regular ANF structures with the corresponding FLL-based structures, as well as the similarity of the optimized performance proved in the previous section, the analysis presented hereafter has been specifically focused on the FLL-equivalent architectures only.

The performance evaluation tests are conducted via simulation, with the same setup introduced previously. In addition, an 8th order Butterworth FE filter, with 20.46 MHz pass-band is employed, while no Analog-to-Digital Converter (ADC) is adopted to intentionally preserve the signal full dynamic with no quantization losses. The signal and noise density powers are set respectively to $P_C = -146.3$ dBW and $N_0 = -201.3$ dBW/Hz, resulting in a carrier to noise ratio C/N_0 of 55 dB-Hz. A wide-sweep slow rate jamming signal, whose features are reported in Section II, is then added to the baseband complex envelope of the clean signal: three jamming powers $P_J = \{-130, -110, -103\}$ dBW are considered to simulate respectively a weak, medium and strong jammer scenarios, resulting in $J/N = \{-1.8, 18.2, 25.2\}$ dB and $J/S = \{16.3, 36.3, 43.3\}$ dB.

The generated signal is given as input to the MATLAB® model of the FLL-equivalent ANFs, as detailed in Section III, using equations (6) and (8) for the notch filter and the adaptation algorithms described in Table 4. The filtered signal is finally processed by a MATLAB®-based GNSS software receiver, where only the acquisition stage is enabled. An FFT-based Parallel Code Phase Search Acquisition is adopted, with integration time $T_{int} = 1$ ms, one coherent/non-coherent sums and false alarm probability $P_{fa} = 0.001$. The α_{mean} metric is evaluated according to (15) and averaged along 50 ms total signal length.

Figure 9 reports the α_{mean} evaluation for the three considered jamming scenarios for both the exponential filtering FLL (Figure 9-(a), (c) and (e)) and the standard FLL (Figure 9-(b), (d) and (f)). In particular, the top subplot shows α_{mean} as a function of the pole contraction factor k_α and the loop bandwidth B_n, while the bottom one illustrates the successful acquisition percentage γ, defined as the total percentage of time in which the signal has been successfully acquired. The grey dashed line and grey bars are used for the unfiltered signal (ANF disabled), as reference, while all other colors represent the filtered signal (one color per loop bandwidth B_n). For the readers' convenience, the best combination of k_α and B_n, i.e. the one achieving the maximum α_{mean}, is reported. A summary of the performance comparison is also shown in Table 5, where α_{mean} measurements in case of the filtered signal, using the best parameters setup of the FLL-equivalent ANFs, are evaluated against the unfiltered case for the three J/N conditions mentioned above. In particular, the third row in Table 5 lists the α_{mean} when the ANF is disabled, while the fourth and

fifth rows contain those achieved with exponential FLL and standard FLL respectively. For both algorithms the percentage improvement with respect to the unfiltered case is also indicated in brackets.

As shown in Figure 9-(a) and (b), the filtering is not really necessary in case of weak jamming power, as expected. Indeed, as clearly pointed out by the grey bars in the bottom plots of Figure 9-(a) and (b), the GNSS signal is always successfully acquired even when the ANF is disabled. The successful acquisition percentage results are also showing that when the ANF is active for $k_\alpha > 0.2$ in Figure 9-(a) and $k_\alpha > 0.3$ in Figure 9-(b), the filtered signal is acquired for all the considered loop bandwidths with 100 % rate. The ANF effectiveness become evident when a significant increase of α_{mean} with respect to the unfiltered case can be measured. In this regard, the exponential FLL shows to be effective for $0.7 < k_\alpha < 0.9$ and $B_n > 6$ MHz with a maximum improvement of 1.92 dB (4.4 % in Table 5) for the best parameters combination, i.e. ${k_\alpha}^{best} = 0.8$ and ${B_n}^{best} = 12$ MHz. On the contrary, the standard FLL cannot be considered really effective. Anyway, for the best parameters choice, i.e. ${k_\alpha}^{best} = 0.9$ and ${B_n}^{best} = 4$ MHz, performances are comparable with those when the ANF is disabled, with a negligible α_{mean} degradation (-0.6 % in Table 5).

A remarkable α_{mean} improvement is instead observed for medium and strong jamming powers, as clearly appears in Figure 9-(c), (d), (e) and (f). In all these cases, the ANF is fundamental. Without it, the acquisition is almost impossible, as shown in the bar graphs. Differently from the weak jammer condition, in these cases all the values of k_α and B_n are able to provide an improved α_{mean}, meaning that the filtering is beneficial whatever the amount of filtered power. In this regard, the colored bars clearly show a slight reduction of the useful k_α range for an increasing jamming power. Focusing on the worst case, i.e. $J/N = 25.2$ dB in Figure 9-(e) and (f), optimal γ are obtained for all the considered loop bandwidths when k_α is in the range $[0.5 - 0.8]$. On the other hand, since the notch rejection bandwidth $B_{3dB} \approx (1 - k_\alpha) f_s/\pi$ [25], small values of k_α are not recommended, in order to keep the notch bandwidth as narrow as possible, thus preserving the useful GNSS signal. We can also notice that for $k_\alpha > 0.8$, the exponential FLL performance is significantly much degraded for low bandwidths, namely $B_n < 6$ MHz, with respect to the standard FLL (see the top subplots in Figure 9-(e) and (f)). This is in line with findings in [15], where it has been shown that for the exponential filtering FLL the pole contraction factor also determines the decay rate of the exponential filter, namely the bigger k_α the slower the filter will be, thus requiring higher B_n to increase its reactivity.

In Table 5 the exponential and standard FLLs get maximum α_{mean} improvement of 89.1 % and 92.3 % respectively for a medium jammer power. In case of strong jammer, such improvement slightly decreases to 68.7 % and 75.1 % respectively. Furthermore, the standard FLL overcomes the exponential FLL for medium-strong jammer with about 3 % and 6 % advantage, while showing a 5 % degradation for weak jamming signal. While the former situation finds explanation in the faster reactivity of the standard FLL to the frequency discontinuities produced by the jammer, as pointed out in [15], the latter has to be likely searched in the adaptation rule. Minimizing the MA output provides a better tracking performance at the price of reducing the capability of discriminating the interference signal from the useful one: this becomes particularly relevant for lower J/N situations.

According to the above analysis and as a general observation, all these results clearly demonstrate that the pole contraction factor is the only parameter having a significant impact on the α_{mean} metric, while the loop bandwidth does not have a noteworthy effect. This could be partly explained by the objective of the acquisition stage: a rough estimation of the code delay and Doppler frequency. More relevant differences are expected in the tracking stage, where such estimation has to be refined in order to lock the GNSS signal.

Accepting a small degradation for low J/N conditions, $k_\alpha = 0.8$ seems to be a good choice for both the FLL models, while $4 \text{ MHz} \leq B_n \leq 6$ MHz and $8 \text{ MHz} \leq B_n \leq 12$ MHz are recommended for the standard FLL and the exponential FLL respectively. This further supports the findings in [15]: the standard FLL requires smaller loop bandwidths, thus implying less noise entering the system and consequently lower frequency jitter (standard deviation of the notch frequency error).

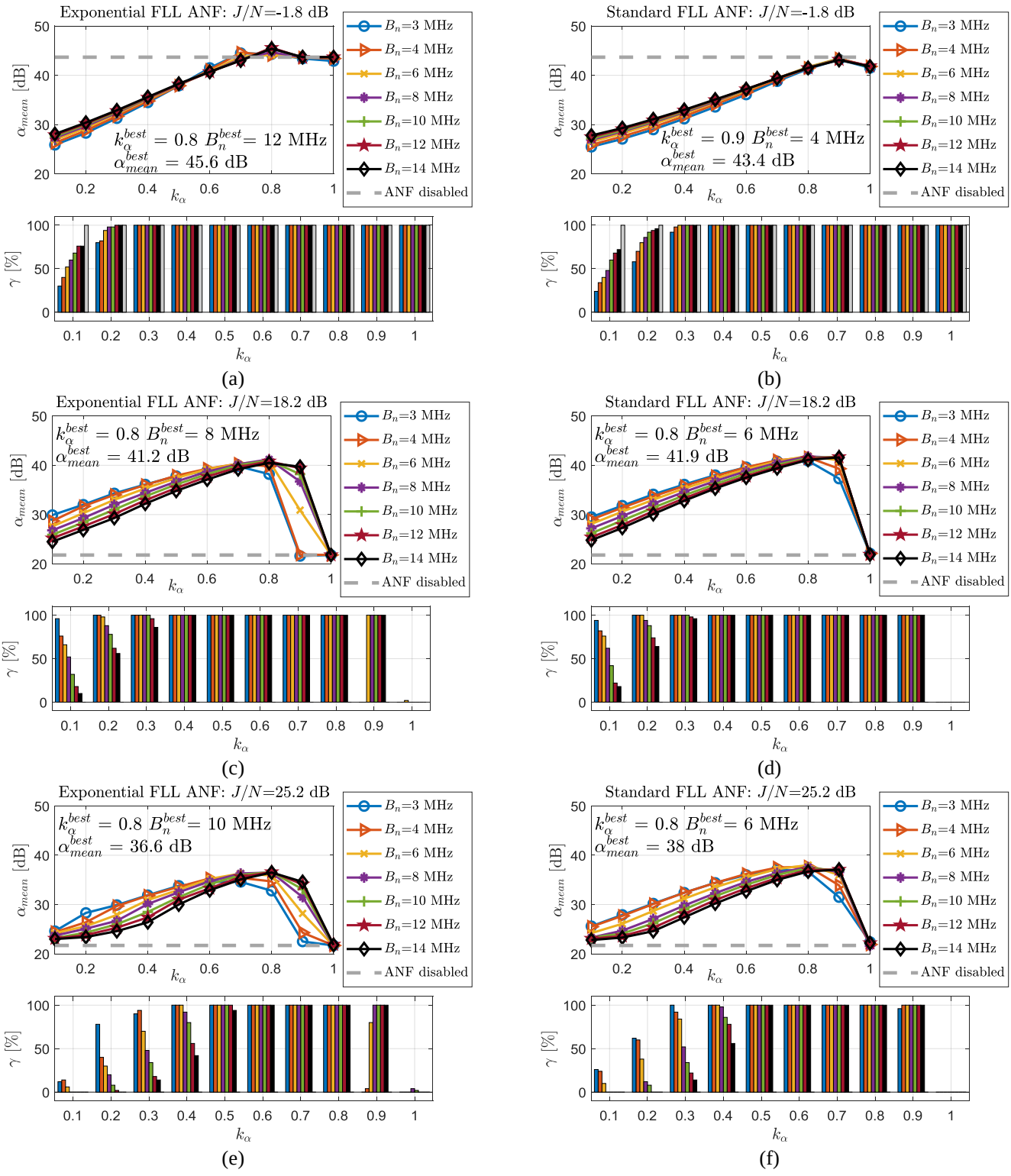

Figure 9. α_{mean} and successful acquisition percentage γ evaluated as a function of the pole contraction factor k_α and the loop bandwidth B_n for the standard FLL and the exponential FLL ANFs respectively in case of $J/N = -1.8$ dB (a)(b), $J/N = 18.2$ dB (c)(d) and $J/N = 25.2$ dB (e)(f). Constant $C/N_0 = 55$ dB $-$ Hz is considered.

Table 5. Comparison of α_{mean} measured for the signal filtered, using the FLL-equivalent ANFs with the best parameter settings, against the unfiltered case for several J/N conditions.

FLL-equivalent ANFs		J/N (dB)		
		-1.8	**18.2**	**25.2**
ANF disabled	α_{mean} (dB):	43.68	21.79	21.7
Exponential FLL with best (k_α, B_n) combination	α_{mean} (dB): (% gain)	45.6 (4.4 %)	41.2 (89.1 %)	36.6 (68.7 %)
Standard FLL with best (k_α, B_n) combination	α_{mean} (dB): (% gain)	43.4 (-0.6 %)	41.9 (92.3 %)	38 (75.1 %)

V. CONCLUSIONS AND FUTURE WORK

In this paper, four ANF architectures have been compared in terms of distortion induced by the filtering operation on the GNSS ranging code in case of swept-frequency (chirp) jamming signals. The adopted methodology is based on the α_{mean} metric evaluated in the acquisition stage of a GNSS receiver for different parameter settings and different J/N conditions. The obtained results showed that, with the best configuration of parameters, i.e. the one maximizing α_{mean}, the four architectures basically achieve similar performance.

The α_{mean} evaluation is a first valid instrument to choose the best configuration setup for the ANF in order to maximize the acquisition performance. Anyway, a fair parameters optimization has to be performed taking into account other key metrics along the whole GNSS signal processing chain. For instance, the tracking stage performance needs to be evaluated in order to complete the distortion analysis. In this regard, the work conducted in [12] on a model of exponential FLL ANF to assess correlation distortions in the GNSS signal tracking loop could be extended to all other architectures considered above. This is expected to be performed in the next future in order to integrate and accomplish the methodology framework.

In addition to this, the parameters optimization is recommended to be repeated on the final ANF implementation and test setup: the implementation of such interference mitigation techniques on a real receiver implies practical aspects having an impact on the performance. For instance, a trade-off between filtering performance and computational load has to be considered depending on the target implementation (hardware/software, floating point/fixed-point precision, real-time/post-processing). In [12] the FPGA implementation of an ANF required the introduction of computational approximations at the price of performance degradation. Furthermore, the bandwidth limitation and quantization effects of the employed front-end have to be carefully considered. Such limitations introduce quantization losses and saturation effects, able to modify the input signal. In this regards, as shown in [26], a jamming signal can be perceived as a form of pulsed interference if the front-end bandwidth is much narrower than the jamming one. In such case, the ANF behavior has to be verified and also other more suitable solutions, e.g. the pulse blanking, have to be evaluated. Finally, as pointed out in [1][12][26], a high number of bits of the ADC is highly recommended for interference mitigation purposes, in order to enhance the recovery of the useful GNSS signal after the filtering operation.

ACKNOWLEDGMENTS

The work of Micaela Troglia Gamba and Emanuela Falletti has been partially funded by the ASTRail project. This project received funding from the Shift2Rail Joint Undertaking under the European Union's Horizon 2020 research and innovation programme under grant agreement No 777561. The content of this paper reflects only the authors' view and the Shift2Rail Joint Undertaking is not responsible for any use that may be made of the included information.

The work of Wenjian Qin is under the TREASURE project funded by the European Union's Horizon 2020 research and innovation programme under the Marie Skodowska-Curie Actions grant agreement No 722023.

REFERENCES

[1] Dovis, F., Ed., *GNSS Interference Threats & Countermeasures*. Norwood, MA, USA: Artech House, 2015.

[2] Curran, J. T., Bavard, M., Closas, P., and Navarro, M., A Look at the Threat of Systematic Jamming of GNSS, Inside GNSS Magazine, September/October 2017.

[3] Rogoway, T., USAF is Jamming GPS in the Western U.S. for Largest Ever Red Flag Air War Exercise, The Drive Magazine, January 2018.

[4] Nott, G., Qld Cops Aim High with Signal Jamming Drone Guns, CIO Magazine, February 2018.

[5] Military Drones Prove Vulnerable to GPS Jamming, The Maritime Executive Magazine, April 2018.

[6] Borio, D., and Closas, P., A Fresh Look at GNSS Anti-Jamming, Inside GNSS Magazine, September/October 2017.

[7] Fadaei, N., Detection, Characterization and Mitigation of GNSS Jamming Interference Using Pre-Correlation Methods, Master of Science Thesis, University of Calgary, April 2016.

[8] Thombre, S., et al., "GNSS Threat Monitoring and Reporting: Past, Present, and a Proposed Future," *The Journal of Navigation*, Vol. 71, No. 3, 2017, pp. 513-529.

[9] Borio, D., "Loop Analysis of Adaptive Notch Filters," *IET Signal Processing*, Vol. 10, No. 6, August 2016, pp. 659-669.

[10] Amin, M. G., Borio, D., Zhang, Y. D., and Galleani, L., "Time-Frequency Analysis for GNSSs: From Interference Mitigation to System Monitoring," *IEEE Signal Processing Magazine*, Vol. 34, No. 5, September 2017, pp. 85-95.

[11] Borio, D., Camoriano, L., and Lo Presti, L., "Two-Pole and Multi-Pole Notch Filters: A Computationally Effective Solution for GNSS Interference Detection and Mitigation," *IEEE Systems Journal*, Vol. 2, No. 1, March 2008, pp. 38-47.

[12] Troglia Gamba, M., Falletti, E., Rovelli, D., and Tuozzi, A., "FPGA Implementation Issues of a Two-pole Adaptive Notch Filter for GPS/Galileo Receivers," *Proceedings of the 25th International Technical Meeting of The Satellite Division of the Institute of Navigation (ION GNSS 2012)*, Nashville, TN, September 2012, pp. 3549–3557.

[13] Nguyen, T. T., The, V. L., Ta, T. H., Nguyen, H. L. T., Motella, B., "An Adaptive Bandwidth Notch Filter for GNSS Narrowband Interference Mitigation", *Journal on Electronics and Communications*, Vol. 4, No. 3-4, July-December 2014.

[14] Borio, D., O'Driscoll, C., and Fortuny, J., "GNSS Jammers: Effects and Countermeasures," *2012 6th ESA Workshop on Satellite Navigation Technologies (NAVITEC 2012)*, Noordwijk, Netherlands, December 2012, pp. 1-7.

[15] Troglia Gamba, M., and Falletti, E., "Performance Analysis of FLL Schemes to Track Swept Jammers in an Adaptive Notch Filter," accepted to be presented at the *2018 9th ESA Workshop on Satellite Navigation Technologies (NAVITEC 2018)*, Noordwijk, Netherlands, December 2018.

[16] Mitch, R. H., et al., "Signal Characteristics of Civil GPS Jammers," *Proceedings of the 24th International Technical Meeting of The Satellite Division of the Institute of Navigation (ION GNSS 2011)*, Portland, OR, September 2011, pp. 1907-1919.

[17] D4.2: Draft Standards for Receiver Testing Against Threats, STRIKE3 Public Deliverable, Issue 2.0, November 2017.

[18] Borio, D., Camoriano, L., Presti, L. L., and Mulassano, P., "Analysis of the One-pole Notch Filter for Interference Mitigation: Wiener Solution and Loss Estimations," *Proceedings of the 19th International Technical Meeting of the Satellite Division of The Institute of Navigation (ION GNSS 2006)*, Fort Worth, TX, September 2006, pp. 1849–1860.

[19] Calmettes, V., Pradeilles, F., and Bousquet, M.: "Study and Comparison of Interference Mitigation Techniques for GPS Receiver," *Proceedings of the 14th International Technical Meeting of the Satellite Division of The Institute of Navigation (ION GPS 2001)*, Salt Lake City, UT, September 2001, pp. 957-968.

[20] Borio, D., A Statistical Theory for GNSS Signal Acquisition. Ph.D. Dissertation, Politecnico di Torino, April 2008.

[21] Choi, J.W., and Cho, N. I., "Suppression of Narrow-band Interference in DS-spread Spectrum Systems Using Adaptive IIR Notch Filter," *Elsevier Signal Processing*, Vol. 82, No. 12, December 2002, pp. 2003-2013.

[22] Falletti, E., Margaria, D., and Motella, B., "A Complete Educational Library of GNSS Signals and Analysis Functions for Navigation Studies," *Coordinates*, Vol. V, No. 8, August 2009, pp. 30-34.

[23] Margaria, D., Falletti, E., Motella, B., Pini, M., and Povero, G., "N-FUELS, a GNSS Educational Tool for Simulation and Analysis of a Variety of Signals in Space," *Proceedings of the European Navigation Conference on GNSS, ENC-GNSS 2010*, Braunschweig, Germany, October 2010.

[24] Stephens, S. A. and Thomas, J. B., "Controlled-root Formulation for Digital Phase-locked Loops," *IEEE Transactions on Aerospace and Electronic Systems*, Vol. 31, No. 1, January 1995, pp. 78-95.

[25] Abdizadeh, M., GNSS Signal Acquisition in The Presence of Narrowband Interference, Ph.D. Dissertation, University of Calgary, September 2013.

[26] Borio, D., "Swept GNSS Jamming Mitigation Through Pulse Blanking," *2016 European Navigation Conference (ENC)*, Helsinki, 2016, pp. 1-8.